Nordstrom, D.K. and Munoz, J.L. 1986. *Geochemical Thermodynamics*. Palo Alto, Blackwell Scientific.
Saxena, S.K., Chaterjee, N., Fei, Y. and Shen, G. 1993. *Thermodynamic Data on Oxides and Silicates*. Berlin, Springer Verlag.

PROBLEMS

1. Consider the following minerals:

anhydrite: $CaSO_4$
bassanite: $CaSO_4.½H_2O$ (the stuff of which plaster of paris is made)
gypsum: $CaSO_4.2H_2O$

(**a**) If water vapor is the only phase of pure water in the system, how many phases are there in this system and how many components are there?
(**b**) How many phases are present at invariant points in such a system? How many univariant reactions are possible? Write all univariant reactions, labeling each according the phase that does not participate in the reaction.

2. Consider a system consisting of olivine of variable composition ($(Mg,Fe)_2SiO_4$) and orthopyroxene of variable composition ($(Mg,Fe)SiO_3$). What is the *minimum* number of components needed to describe this system?

3. In section 3.2.1.3, we showed that a system containing H_2O, H_2CO_3, HCO_3^-, CO_3^{2-}, H^+, and OH^- could be described in terms of components CO_3^{2-}, H^+, and OH^-. Find a different set of components that describe the system equally well. Show that each of the species in the system is an algebraic sum of your chosen components.

4. Use the data in Table 2.2 to construct a temperature-pressure phase diagram that showing the stability fields of calcite and aragonite.

5. Consider the following hypothetical gaseous solution: gases 1 and 2 form an ideal binary solution; at 1000 K, the free energies of formation from the elements are –50 kJ/mol for species 1 and –60 kJ/mol for species 2.

(**a**) Calculate ΔG_{mixing} for the solution at 0.1 increments of X_2. Plot your results.
(**b**) Calculate $\bar{G}$ for an *ideal* solution at 0.1 increments of X_2. Plot your results.
(**c**) Using the method of intercepts, find μ^1 and μ^2 in the solution at $X_2 = 0.2$

6. Using the thermodynamic data in Table 2.2, determine which side of this reaction is stable at 600°C and 400 MPa.:

$$2Al(OH)_3 \rightleftharpoons Al_2O_3 + 3H_2O$$

7. The following analysis of water is from the Rhine River as it leaves the Swiss Alps:

HCO_3^-	113.5 ppm	SO_4^-	36.0 ppm
Cl^-	1.1 ppm	NO_3^-	1.9 ppm
Ca^{2+}	40.7 ppm	Mg^{2+}	7.2 ppm
Na^+	1.4 ppm	K^+	1.2 ppm

(**a**) Calculate the ionic strength of this water. (Recall that concentrations in ppm are equal to concentrations in mmol kg^{-1} multiplied by formula weight.)
(**b**) Using the Debye–Hückel equation and the data in Table 3.2, calculate the practical activity coefficients for each of these species at 25°C.

8. Seawater has the following composition:

Na^+	0.481 M
Mg^{2+}	0.0544 M
Ca^{2+}	0.0105 M
K^+	0.0105 M
Cl^-	0.560 M
SO_4^-	0.0283 M
HCO_3^-	0.00238 M

(a) Calculate the ionic strength.
(b) Using the Davies equation and the data in Table 3.2, calculate the practical activity coefficients for each of these species at 25°C.

9. The following is an analysis of *Acqua di Nepi*, a spring water from the Italian province of Viterbo:

HCO_3^-	451 ppm	SO_4^{2-}	38 ppm
Cl^-	20 ppm	NO_3^-	9 ppm
Ca^{2+}	82 ppm	Mg^{2+}	27 ppm
Na^+	28 ppm	K^+	50 ppm
F^-	1.3 ppm		

(a) Calculate the ionic strength of this water.
(b) Using the Debye–Hückel equation and the data in Table 3.1, calculate the practical activity coefficients for each of these species at 25°C.

10. Water from Thonon, France has the following composition:

Anions	mg/l	Cations	mg/l
HCO_3^-	332	Ca^{2+}	103.2
SO_4^{2-}	14	Mg^{2+}	16.1
NO_3^-	14	K^+	1.4
Cl^-	8.2	Na^+	5.1

(a) What is the ionic strength of this water?
(b) What are the activity coefficients for HCO_3^- and CO_3^{2-} in this water?
(c) Assuming an equilibrium constant for the dissociation of bicarbonate:

$$HCO_3^- \rightleftharpoons H^+ + CO_3^-$$

of 4.68×10^{-11} and a pH of 7.3, what is the equilibrium concentration of CO_3^{2-} in this water?

11. The equilibrium constant for the dissolution of galena:

$$PbS_{solid} + 2H^+ \rightleftharpoons Pb^{2+}_{aq} + H_2S^{aq}$$

is 9.12×10^{-7} at 80°C. Using $\gamma_{Pb^{2+}} = 0.11$ and $\gamma_{H2S} = 1.77$, calculate the equilibrium concentration of Pb^{2+} in aqueous solution at this temperature and at pHs of 6, 5 and 4. Assume the dissolution of galena is the only source of Pb and H_2S in the solution, and that there is no significant dissociation of H_2S. *Hint:* mass balance requires that $[H_2S] = [Pb^{2+}]$.

12. The dissociation constant for hydrofluoric acid (HF) is $10^{-3.2}$ at 25°C. What would be the pH of a 0.1 M solution of HF? You may assume ideal behavior. (*Hint*: Ask yourself what addition constraints are imposed on the system. Your final answer will require solving a quadratic equation.)

13. The first dissociation constant for H_2S is $K_1 = 9.1 \times 10^{-3}$. Neglecting the second dissociation and assuming ideality (i.e. activity equals concentration), what is the pH of 1 liter of pure water if you dissolve 0.01 moles of H_2S in it? What fraction of H_2S has dissociated? *(HINT: assume that the concentration of OH^- is negligible (in other words, no autodissociation of water) and use the quadratic equation for your final solution.)*

14. Given the following analysis of biotite and assuming a *mixing-on-site model* for all sites, calculate the activities of the following components:

$$KMg_3Si_3AlO_{10}(F)_2 \text{ (fluorophlogopite)}$$

$$KFe_3^{+2}Si_3AlO_{10}(OH)_2 \text{ (annite)}$$

Site	Ion	Ions per site
Tetrahedral	Si	2.773
	Al	1.227
Octahedral	Al	0.414
	Ti	0.136
	Fe^{+3}	0.085
	Fe^{+2}	1.399
	Mg	0.850
Interlayer	Ca	0.013
	Na	0.063
	K	0.894
Anion	OH	1.687
	F	0.037

Hint: Check your result by making sure the activity of phlogopite in pure phlogopite is 1.

15. Given the following analysis of a pyroxene, use the mixing-on-site model of ideal activities to calculate the activity of *jadeite* ($NaAlSi_2O_6$) and *diopside* ($CaMgSi_2O_6$) in this mineral:

Site	Ion	Ions per site
Tetrahedral	Si	1.96
	Al	0.04
Octahedral M1	Al	0.12
	Mg	0.88
Octahedral M2	Fe	0.06
	Ca	0.82
	Na	0.12

16. Write the equilibrium constant expression for the reaction:

$$CaCO_{3(s)} + 2H^+_{(aq)} + SO_4^{2-} + H_2O_{(liq)} \rightleftharpoons CaSO_4 \cdot 2H_2O + CO_{2(g)}$$

assuming the solids are pure crystalline phases and that the gas is ideal.

17. Assuming ideal solution behavior for the following:

(a) Show that the boiling point of a substance is increased when another substance is dissolved in it, assuming the concentration of the solute in the vapor is small.
(b) By how much will the boiling point of water be elevated when 10% salt is dissolved in it?

18. Find $\Delta\bar{G}$ for the reaction:

$$Pb^{2+} + Mn \rightleftharpoons Pb + Mn^{2+}$$

Which side of the reaction is favored? (*HINT: use the data in Table 3.3.*)

19. What is the $\Delta\bar{G}$ for the reaction:

$$Cu^{2+} + e^{-} \rightleftharpoons Cu^{+}$$

What is the $p\varepsilon^\circ$ for this reaction?

20. Consider a stream with a pH of 6.7 and a total dissolved Fe concentration of 1 mg/l. Assume ideal behavior for this problem.

(a) If the stream water is in equilibrium with the atmospheric O_2 (partial pressure of 0.2 MPa), what is the pε of the water?
(b) Assuming they are the only species of Fe in the water, what are the concentrations of Fe^{3+} and Fe^{2+}? Use the pε you determined in part a.

21. Write reactions for the oxidation of nitrogen gas to aqueous nitrite and nitrate ions that contain the electron and hydrogen ion (i.e., reactions suitable for a pε–pH diagram). Write the log equilibrium constant expression for these reactions. Using the data below, calculate the log equilibrium constant for these reactions under standard state conditions). Calculate $p\varepsilon^\circ$ and E_H^o for these reactions. *Hint*: remember, in the standard state, *all* reactants and products have activities of 1.

Species	ΔG_f^o kJ/mol
H_2O	–237.19
N_2 (gas)	0
NO_3^-	–111.3
NO_2^-	–32.2

Standard state is 25°C and 0.1 MPa. R = 8.314 J/mol-K.

22. Construct a pε–pH diagram for the following species of sulfur: HSO_4^-, SO_4, H_2S, HS^-, and S^{2-} at 25°C and 0.1 MPa. The following free energies of formation should provide sufficient information to complete this task.

Species	ΔG_f°	Species	ΔG_f°
S^{2-} (aq)	+85.81	H_2O	–237.19
HS^- (aq)	+12.09	H^+	0
H_2S (aq)	–27.82	H_2 (g)	0
SO_4^{2-} (aq)	–744.54	O_2 (g)	0
HSO_4^- (aq)	–755.92		

Values are in kJ/mol, standard state is 25°C and 0.1 MPa. R = 8.314 J/mol-K.

23. Construct a pε–pH diagram for dissolved species of uranium, UO_2^{2+} and $U(OH)_5^-$, and the two solid phases UO_2 and U_3O_8 at 25°C and 0.1 MPa. Assume the activity of dissolved uranium is fixed at 10^{-6}. The following free energies of formation should provide sufficient information to complete this task.

Species	ΔG_f^o
$U(OH)_5^-$ (aq)	–1630.80
UO_2^{2+} (aq)	–952.53
UO_2 (s)	–1031.86
U_3O_8 (s)	–3369.58
H_2O	–237.19

Values are in kJ/mol, standard state is 25°C and 0.1 MPa.
R = 8.314 J/mol-K.

Chapter 4

Applications of thermodynamics to the Earth

4.1 INTRODUCTION

In the previous two chapters, we developed the fundamental thermodynamic relationships and saw how they are applied to geochemical problems. The tools now in our thermodynamic toolbox are sufficient to deal with many geochemical phenomena. They are not sufficient, however, to deal with *all* geochemical phenomena. In this chapter, will add a final few thermodynamic tools. These allow us to deal with non-ideal behavior and exsolution phenomena in solids and silicate liquids. With that, we can use thermodynamics to determine the pressure and temperature at which rock assemblages formed, certainly one of the most useful applications of thermodynamics to geology. Along the way, we will see how thermodynamics is related to one of the most useful tools in petrology: phase diagrams. We will then briefly consider how thermodynamics has been used to construct computer models of how magma compositions evolve during melting and crystallization. Finally, we return to the question of non-ideal behavior in electrolyte solutions and examine in more depth the problems of ion association and solvation and how this affects ion activities. Deviations from ideal behavior tend to be greater in solutions of high ionic strength, which includes such geologically important solutions as hydrothermal and ore-forming fluids, saline lake waters, metamorphic fluids, and formation and oil field brines. We briefly examine methods of computing activity coefficients at ionic strengths relevant to such fluids.

4.2 ACTIVITIES IN NON-IDEAL SOLID SOLUTIONS

4.2.1 Mathematical models of real solutions: Margules equations

Ideal solution models often fail to describe the behavior of real solutions; a good example is water and alcohol, as we saw in Chapter 3. Ideal solutions fail spectacularly when exsolution occurs, such as between oil and vinegar, or between orthoclase and albite, a phenomenon we will discuss in more detail shortly. In non-ideal solutions, even when exsolution does not occur, more complex models are necessary.

Power, or Maclaurin, series are often a convenient means of expressing complex mathematical functions, particularly if the true form of the function is not known, as is often the case. This approach is the basis of Margules* equations, a common method of calculating excess state functions. For example, we could express the excess volume as a power series:

$$\bar{V}_{ex} = A + BX_2 + CX_2^2 + DX_2^3 + \ldots \quad (4.1)$$

where X_2 is the mole fraction of component 2.

* Named for Max Margules (1856–1920), an Austrian meteorologist, who first used this approach in 1895.

Geochemistry, First Edition. William M. White.

Following the work of Thompson (1967), Margules equations are used extensively in geochemistry and mineralogy as models for the behavior of non-ideal solid solutions. It should be emphasized that this approach is completely empirical – true thermodynamic functions are not generally power series. The approach is successful, however, because nearly any function can be *approximated* as a power series. Thus Margules equations are attempts to approximate thermodynamic properties from empirical observations when the true mathematical representation is not known. We will consider two variants of them: the symmetric and asymmetric solution models.

4.2.1.1 The symmetric solution model

In some solutions, a sufficient approximation of thermodynamic functions can often be obtained by using only a second-order power series (i.e., in eqn. 4.1, $D = E = \ldots = 0$). Now in a binary solution, the excess of any thermodynamic function should be entirely a function of mole fraction X_2 (or X_1, however we wish to express it). Put another way, where $X_2 = 0$, we expect $\bar{V}_{ex} = 0$. From this we can see that the first term in eqn. 4.1, A, must also be 0. Thus eqn. 4.1 simplifies to:

$$\bar{V}_{ex} = BX_2 + CX_2^2 \tag{4.2}$$

The simplest solution of this type would be one that is symmetric about the midpoint, $X_2 = 0.5$; this is called a *symmetric solution*. In essence, symmetry requires that:

$$BX_2 + CX_2^2 = BX_1 + CX_1^2 \tag{4.3}$$

Substituting $(1 - X_2)$ for X_1 and expanding the right-hand side of eqn. 4.3, we have:

$$BX_2 + CX_2^2 = B - BX_2 + C - 2CX_2 + CX_2^2 \tag{4.4}$$

Collecting terms and rearranging:

$$B(2X_2 - 1) = C(1 - 2X_2) \tag{4.5}$$

which reduces to $B = -C$. Letting $W_V = B$ in eqn. 4.2, we have:

$$\begin{aligned} V_{ex} &= W_V X_2 - W_V X_2^2 = W_V X_2 (1 - X_2) \\ &= X_1 X_2 W_V \end{aligned} \tag{4.6}$$

W is known as an *interaction parameter* because non-ideal behavior arises from *interactions* between molecules or atoms and depends on temperature, pressure, and the nature of the solution, but not on X. Expressions similar to 4.2–4.6 may be written for enthalpy, entropy, and free energy; for example:

$$\bar{G}_{ex} = X_1 X_2 W_G \tag{4.7}$$

The W_G term may be expressed as:

$$W_G = W_U + PW_V - TW_S \tag{4.8}$$

Since the W_H term can be written as:

$$W_H = W_U + PW_V$$

then eqn. 4.8 may also be written:

$$W_G = W_H - TW_S \tag{4.8a}$$

The temperature and pressure dependence of W_G are then

$$\left(\frac{\partial W_G}{\partial T}\right)_P = -W_s \tag{4.9}$$

$$\left(\frac{\partial W_G}{\partial P}\right)_T = W_V \tag{4.10}$$

*Regular solutions** are a special case of symmetric solutions where:

$$W_s = 0 \quad \text{and therefore} \quad W_G = W_H$$

Regular solutions correspond to the case where $\Delta S_{ex} = 0$, i.e., where $\Delta S_{mixing} = \Delta S_{ideal}$, and therefore where $W_S = 0$. From eqn. 4.9, we see that W_G is independent of temperature for regular solutions. Examples of such solutions include electrolytes with a single, uncoupled, anionic or cationic substitution, such as $CaCl_2$–$CaBr_2$, or solid solutions where there

* The term regular solution is often used to refer to symmetric solutions. In that case, what we termed a regular solution is called a *strictly regular solution*.

is a single substitution in just one site (e.g., Mg_2SiO_4–Fe_2SiO_4).

Setting eqn. 4.7 equal to eqn. 3.57, we have for binary solutions:

$$\bar{G}_{ex} = X_1X_2W_G = RT[X_1 \ln \lambda_1 + X_2 \ln \lambda_2] \quad (4.11)$$

For a symmetric solution we have the additional constraint that at $X_2 = X_1$, $\lambda_1 = \lambda_2$. From this relationship it follows that:

$$RT \ln \lambda_i = X_j^2 W_G \quad (4.12)$$

This leads to the relationships:

$$\mu_1 = \mu_1^o + RT \ln X_1 + X_2^2 W_G \quad (4.13)$$

$$\mu_2 = \mu_2^o + RT \ln X_2 + X_1^2 W_G \quad (4.13a)$$

The symmetric solution model should reduce to Raoult's and Henry's laws in the pure substance and infinitely dilute solution respectively. We see that as $X_1 \rightarrow 1$, eqns. 4.13 and 4.13a reduce respectively to:

$$\mu_1 = \mu_1^o + RT \ln X_1 \quad (4.14)$$

$$\mu_2 = \mu_2^o + RT \ln X_2 + W_G \quad (4.15)$$

Equation 4.14 is Raoult's Law; letting:

$$\mu^* = \mu^\circ + W_G \quad \text{or} \quad W_G = RT \ln h$$

then eqn. 4.15 is Henry's Law. Thus the interaction parameter can be related to the parameters of Henry's Law, and activity coefficient. In the Margules representation, a solution that is ideal throughout is simply the special case where $A = B = C = D = \ldots = 0$.

4.2.1.2 *The asymmetric solution model*

Many real solutions, for example mineral solutions with asymmetric solvi, are not symmetric. This corresponds to the case where D in eqn. 4.1 is non-zero, so we must carry the expansion to the third order. It can be shown that in this case the excess free energy in binary solutions is given by:

$$\bar{G}_{ex} = (W_{G_1} X_2 + W_{G_2} X_1) X_1 X_2 \quad (4.16)$$

(You can satisfy yourself that this may be written as a power series to the third order of either X_1 or X_2.) The two coefficients are related to the Henry's Law constants:

$$W_{G_i} = \mu_i^* - \mu_i^o = RT \ln h_i \quad (4.17)$$

Activity coefficients are given by:

$$\nu RT \ln \lambda_i = (2W_{G_j} - W_{G_i})X_j^2 + 2(W_{G_i} - W_{G_j})X_j^3 \quad (4.18)$$

where $j = 2$ when $i = 1$ and vice versa, and ν is the stoichiometric coefficient. As for the symmetric solution model, the interaction parameters of the asymmetric model can be expressed as the sum of the W_U, W_V, and W_S interaction parameters to account for temperature and pressure dependencies (see Example 4.1).

The alkali feldspars ($NaAlSi_3O_8$–$KAlSi_3O_8$) are an example of a solid solution exhibiting asymmetric exsolution. Figure 4.1 shows the ΔG_{real}, ΔG_{ideal}, and ΔG_{excess} for the alkali feldspar solid solution computed for 600°C and 200 MPa using the asymmetric solution model of Thompson and Waldbaum (1969). ΔG_{excess} is computed from eqn. 4.16, ΔG_{ideal} is computed from eqn. 3.30. Figure 4.2 shows ΔG_{real} for a series of temperatures. Perhaps a clearer picture of how ΔG will vary as a function of both composition and temperature can be obtained by plotting all three variables simultaneously, as in Figure 4.3.

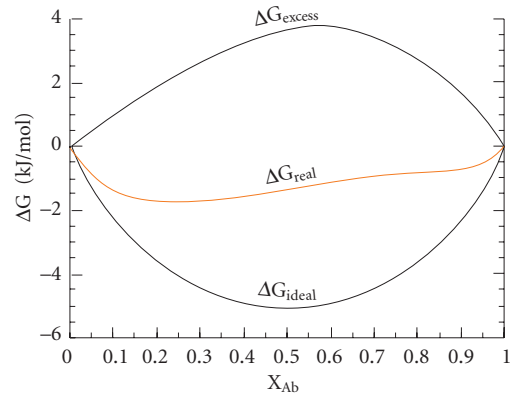

Figure 4.1 Alkali feldspar solid solution computed at 600°C and 200 MPa (2 kb) using the data from Thompson and Waldbaum (1969). $\Delta G_{real} = \Delta G_{ideal} + \Delta G_{excess}$.

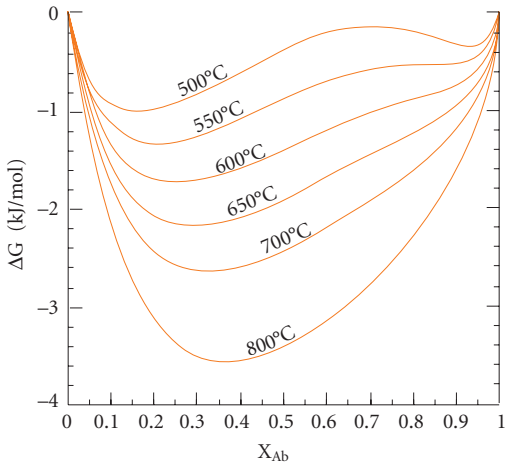

Figure 4.2 ΔG_{real} of alkali feldspar solution computed for a series of temperatures and 200 MPa. From Thompson and Waldbaum (1969).

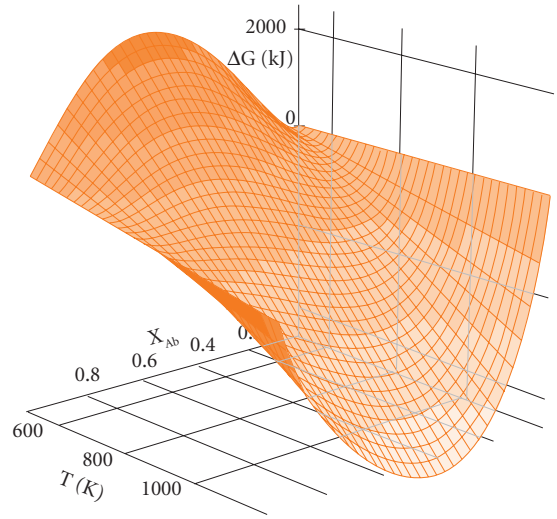

Figure 4.3 ΔG surface for the alkali feldspar solid solution as a function of the mole fraction of albite and temperature. Thompson and Waldbaum (1969).

Example 4.1 Computing activities using Margules parameters

Compute the activity of albite in an albite (Ab) and orthoclase (Or) solid solution (alkali feldspar) as a function of the mole fraction of albite from X_{Ab} = 0 to 1 at 600°C and 200 MPa. Use the asymmetric solution model and the data of Thompson and Waldbaum (1969) given below.

Alkali feldspar Margules parameters

	Ab	Or
W_V (J/MPa-mol)	3.89	4.688
W_S (J/mol)	19.38	16.157
W_H (kJ/mol)	26.485	32.105

Answer: Our first step is to calculate W_G for each end member where $W_G = W_H + W_vP - W_ST$. Doing so, we find W_{GAb} = 10.344 kJ and W_{GOr} = 18.938 kJ. We can then calculate the activity coefficient as a function of X_{Ab} and X_{Or} from eqn. 4.19. The activity is then computed from $a = \lambda X_{Ab}$. The results are plotted in Figure 4.4.

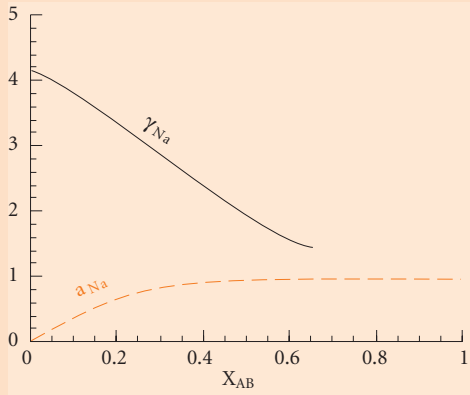

Figure 4.4 Activity and activity cofficient of albite in alkali feldspar solid solution computed at 600°C and 200 MPa using the asymmetric solution model from Thompson and Waldbaum (1969).

4.3 EXSOLUTION PHENOMENA

Now consider a binary system, such as $NaAlSi_3O_8$–$KAlSi_3O_8$ in the earlier example, of components 1 and 2, each of which can form a pure phase, but also together form a solution phase, which we will call *c*. The condition for spontaneous exsolution of components 1 and 2 to form two phases *a* and *b* is simply that $G_a + G_b < G_c$.

As we saw in Chapter 3, the free energy of a real solution can be expressed as the sum of an ideal solution and a non-ideal or excess free energy term:

$$G_{real} = G_{ideal} + G_{ex}$$

The free energy of the ideal part is given by:

$$\bar{G}_{ideal} = \sum_i X_i \mu_i^o + RT \sum_i X_i \ln X_1 \qquad (3.31)$$

Further, the ideal part itself consists of two terms, the first term in eqn. 3.31 corresponding to the free energy of a mechanical mixture ($G_{mixture}$), and the second part being the free energy of ideal mixing ($\Delta G_{ideal\ mixing}$). Figure 4.5a illustrates the variation of G_{excess}, $G_{mixture}$, and G_{ideal} in this hypothetical system. $G_{mixture}$ is simply the free energy of a mechanical mixture of pure components *1* and *2* (e.g., orthoclase and albite). Figure 4.5b illustrates the variation of G_{real} in this system. So long as G_{real} is less than $G_{mixture}$, a solution is stable relative to pure phases *1* and *2*. You can see that G_{ideal} is always less than $G_{mixture}$, so as long as the G_{ex} term is not too great. In the hypothetical case illustrated in Figure 4.5, a solution is always stable relative to a mechanical mixture of the pure end member phases. However, if we look carefully at Figure 4.5b, we see there is yet another possibility, namely that two phases *a* and *b*, each of which is a *limited* solid solution of components 1 and 2, are stable relative to a single solid solution. Thus at equilibrium, two phases will exsolve from the single solution; this is just what occurs at lower temperatures in the alkali feldspar system. It would be useful if thermodynamics could predict when such exsolution will occur. Let's see if our thermodynamics tools are up to the task.

Looking at Figure 4.2, we see that at 800°C, ΔG_{real} defines a continuously concave upward path, while at lower temperatures, such as 600°C (Figure 4.1), inflections occur and there is a region where ΔG_{real} is concave downward. All this suggests we can use calculus to predict exsolution. For a binary

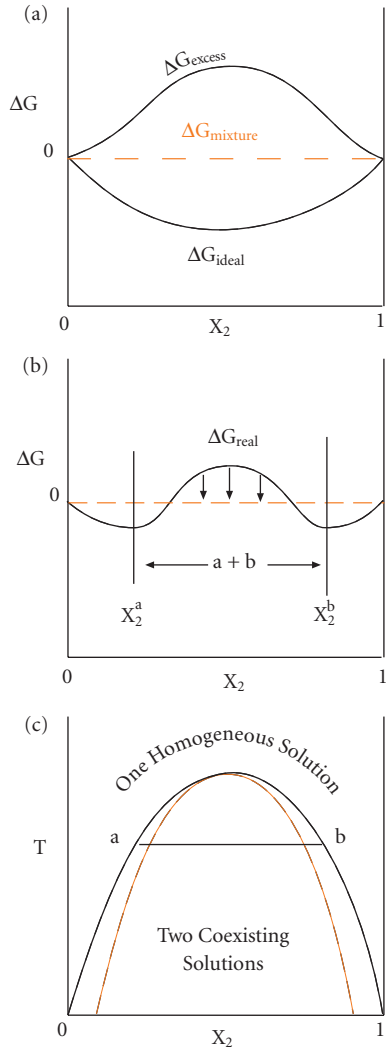

Figure 4.5 (a) Schematic isothermal, isobaric G–X plot for a real solution showing ΔG of mechanical mixing, ideal mixing and excess mixing. (b) Sum of ideal and excess mixing free energies shown in (a). Tangents to the minima give the chemical potentials in immiscible phases *a* and *b*. (c) T–X plot for same system as in (b). Solid line is the *solvus*, red dashed line is the *spinodal*. Exsolution may not occur between the spinodal and solvus because the free energy can locally increase during exsolution. After Nordstrom and Munoz (1986). With permission from John Wiley & Sons.

solution of components 1 and 2, the $G_{mixture}$ and $\Delta G_{ideal\ mixing}$ terms are:

$$G_{mixture} = X_1\mu_1^o + X_2\mu_2^o$$
$$\Delta G_{ideal\ mixing} = RT(X_1 \ln X_1 + X_2 \ln X_2)$$

Equation 3.31 can thus be written as:

$$\bar{G} = X_1\mu_1^o + X_2\mu_2^o + RT(X_1 \ln X_1 + X_2 \ln X_2) + G_{ex} \quad (4.19)$$

Differentiating with respect to X_2 (and recalling that $X_1 = 1 - X_2$), we obtain:

$$\left(\frac{\partial \bar{G}}{\partial X_2}\right) = \mu_2^o - \mu_1^o + RT \ln \frac{X_2}{X_1} + \left(\frac{\partial \bar{G}_{ex}}{\partial X_2}\right) \quad (4.20)$$

This is the equation for the slope of the curve of G vs. X_2. The second derivative is:

$$\left(\frac{\partial^2 \bar{G}}{\partial X_2^2}\right) = \frac{RT}{X_1X_2} + \left(\frac{\partial^2 \bar{G}_{ex}}{\partial X_2^2}\right) \quad (4.21)$$

This tells us how the slope of the curve changes with composition. For an ideal solution, G_{excess} is 0, the second derivative is always positive, and the free energy curve is concave upward. But for real solutions G_{excess} can be positive or negative. If for some combination of T and X (and P), the second derivative of G_{excess} becomes negative and its absolute value is greater than the RT/X_1X_2 term, inflection points appear in the G–X curve. Thus exsolution is thermodynamically favored if for some composition:

$$\frac{RT}{X_1X_2} + \left(\frac{\partial^2 \bar{G}_{ex}}{\partial X_2^2}\right) \leq 0$$

The inflection points occur where the second derivative is 0; however, as may be seen in Figure 4.5b, the inflection points do not correspond with the thermodynamic limits of solubility, which in this diagram are between x_2^a and x_2^b.

We can draw a straight line that is tangent to the free energy curve at x_2^a and x_2^b. This line is the free energy of a mechanical mixture of the two limited solutions *a* and *b*. Phase *a* is mostly component 1, but contains x_2^a of component 2. Similarly, phase *b* is mostly component 2 but contains $1 - x_2^b$ of component 1. The mechanical mixture of *a* and *b* has less free energy than a single solution phase everywhere between x_2^a and x_2^b. It is therefore thermodynamically more stable, so exsolution can occur in this region.

In Figure 4.2, we can see inflection points developing at about 650°C in the alkali feldspar solution. The inflection points become more marked and occur at increasingly different values of X_{Ab} as temperature decreases. The alkali feldspar system illustrates a common situation where there is complete solid solution at higher temperature, but decreasing *miscibility* at lower temperature. This occurs because the free energy of ideal mixing becomes less negative with decreasing temperature (Figure 3.6).

Figure 4.5c shows a schematic drawing of a temperature–composition plot in which there is complete solution at higher temperature with a widening two-phase region at lower temperatures. The boundary between the two-phase and one-phase regions is shown as a solid line and is known as the *solvus*.

The analysis of exsolution is relevant to immiscible liquids (e.g., oil and vinegar, silicate and sulfide melts) as well as solids. There is a difference, however. In solids, exsolution must occur through diffusion of atoms through crystal lattices, while in liquids both diffusion and advection serve to redistribute components in the exsolving phases. As exsolution begins, the exsolving phases begin with the composition of the single solution and must rid themselves of unwanted components. In a solid, this only occurs through diffusion, which is very slow. This leads to a kinetic barrier that often prevents exsolution even though two exsolved phases are more stable than a solution. This is illustrated in Figure 4.6. For example, consider a solution of composition C. It begins to exsolve protophases of A and B, which initially have compositions A′ and B′. Even though a mechanical mixture of A and B will have lower free energy than solution phase C, A′ and B′, the initial products of exsolution, have higher free energy than C. Furthermore, as exsolution proceeds and these phases move toward compositions A and B, this free energy excess becomes larger. Thus exsolution causes a local increase in free energy and therefore cannot occur. This problem is not encountered at composition C′, though, because a mixture of the

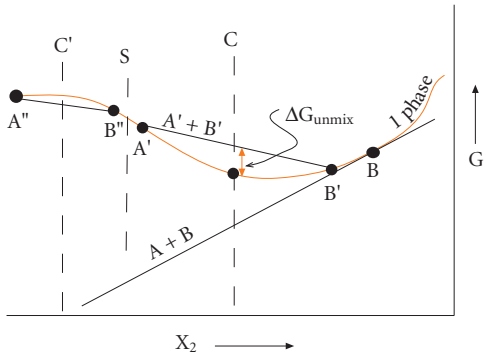

Figure 4.6 A small portion of a *G*–*X* plot illustrating the origin of the spinodal. The process of exsolution of two phases from a single solid solution must overcome an energy barrier. As exsolution from a solution of composition C begins, the two exsolving phases have compositions that move away from C, e.g., A′ and B′. But the free energy of a mechanical mixture of A′ and B′ has greater free energy, by ΔG_{unmix}, than the original single solution phase. Exsolution will therefore be inhibited in this region. This problem does not occur if the original solution has composition C′.

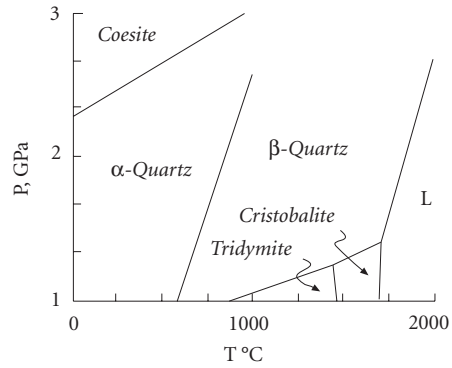

Figure 4.7 P–T phase diagram for SiO_2. This system has one component but 7 phases. L designates the liquid phase. The α–β quartz transition is thought to be partially second-order, that is, it involves only stretching and rotation of bonds rather than a complete reformation of bonds as occurs in first-order phase transitions.

exsolving protophases A″ and B″ has lower free energy than original solution at C′. Thus the actual limit for exsolution is not tangent points such as B but at inflection points (where $\partial^2 G/\partial X^2 = 0$) such as S. The locus of such points is plotted in Figure 4.5c as the red line and is known as the *spinodal*.

4.4 THERMODYNAMICS AND PHASE DIAGRAMS

A *phase diagram* is a representation of the regions of stability of one or more phases as a function of two or more thermodynamic variables such as temperature, pressure, or composition. In other words, if we plot two thermodynamic variables such as temperature and pressure or temperature and composition, we can define an area on this plot where a phase of interest is thermodynamically stable. Figure 4.7 is an example of a T–P phase diagram for a one-component system: SiO_2. The diagram shows the SiO_2 phase stable for a given combination of pressure and temperature. Figure 4.8 is an example of a simple T–X diagram for the two-component system diopside–anorthite ($CaMgSi_2O_6$ or clinopyroxene and Ca-plagioclase, $CaAl_2Si_2O_8$; two of the more common igneous rock-forming minerals). In multicomponent systems we must always be concerned with at least three thermodynamic variables: P, T, and X. Thus any T–X phase diagram will be valid for only one pressure, 0.1 MPa (1 bar ≈ 1 atm) in this case. Of course, with a three-dimensional drawing it is possible to represent both temperature and pressure as well as composition in a binary system.

It should not surprise you at this point to hear that the phase relationships in a chemical system are a function of the thermodynamic properties of that system. Thus phase diagrams, such as Figures 4.7 and 4.8, can be constructed from thermodynamic data. Conversely, thermodynamic information can be deduced from phase diagrams.

Let's now see how we can construct phase diagrams, specifically T–X diagrams, from thermodynamic data. Our most important tool in doing so will be the $\bar{G}$ – X diagrams that we have already encountered. *The guiding rule in constructing phase diagrams from* $\bar{G}$ – X *diagrams is that the stable phases are those that combine to give the lowest* $\bar{G}$. Since a $\bar{G}$ – X diagram is valid for only one particular temperature, we will need a number of $\bar{G}$ – X diagrams at different temperatures to

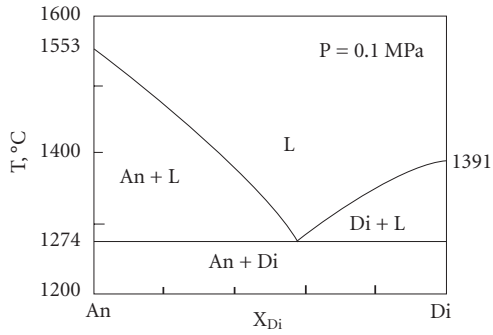

Figure 4.8 Phase diagram (T–X) for the two-component system diopside–anorthite at 1 atm. Four combinations of phases are possible as equilibrium assemblages: liquid (L), liquid plus diopside (L + Di), liquid plus anorthite (L + An), and diopside plus anorthite.

construct a single T–X diagram (we could also construct P–X diagrams from a number of $\bar{G} - X$ diagrams at different pressures). Before we begin, we will briefly consider the thermodynamics of melting in simple systems.

4.4.1 The thermodynamics of melting

One of the more common uses of phase diagrams is the illustration of melting relationships in igneous petrology. Let's consider how our thermodynamic tools can be applied to understanding melting relationships. We begin with melting in a simple one-component system, for example quartz. At the melting point, this system will consist of two phases: a solid and a melt. At the melting point, the liquid and solid are in chemical equilibrium. Therefore, according to eqn. 3.17: $\mu_l = \mu_s$.

The Gibbs free energy of melting, ΔG_m, must be 0 at the melting point (and only at the melting point). Since:

$$\Delta G_m = \Delta H_m - T_m \Delta S_m \qquad (4.22)$$

and $\Delta G_m = 0$ at T_m, then:

$$\Delta H_m = T_m \Delta S_m$$

where ΔH_m is the heat (enthalpy) of melting or fusion,* T_m is the melting temperature, and ΔS_m is the entropy change of melting. Thus the melting temperature of a pure substance is simply:

$$\boxed{T_m = \frac{\Delta H_m}{\Delta S_m}} \qquad (4.23)$$

This is a very simple, but very important, relationship. This equation tells us that temperature of melting of a substance is the ratio of the enthalpy change to entropy change of melting. Also, if we can measure temperature and enthalpy change of the melting reaction, we can calculate the entropy change.

The pressure dependence of the melting point is given by the Clapeyron equation:

$$\frac{dT}{dP} = \frac{\Delta V_m}{\Delta S_m} \qquad (4.24)$$

Precisely similar relationships hold for vaporization (boiling). Indeed, the temperature and pressure boundaries between any two phases, such as quartz and tridymite, calcite and aragonite, and so on, depend on thermodynamic properties in an exactly analogous manner.

In eqn. 3.66 we found that addition of a second component to a pure substance depresses the melting point. Assuming ΔS_m and ΔH_m are independent of temperature, we can express this effect as:

$$\frac{T_{i,m}}{T} = 1 - \frac{R \ln a^{\ell}_{i,m}}{\Delta S_{i,m}} \qquad (4.25)$$

Since enthalpies of fusion, rather than entropies, are the quantities measured, eqn. 4.25 may be more conveniently expressed as:

$$\frac{T_{i,m}}{T} = 1 - \frac{T_{i,m} R \ln a^{\ell}_{i,m}}{\Delta H_{i,m}} \qquad (4.26)$$

Example 4.2 shows how the approximate phase diagram for the diopside–anorthite system (Figure 4.9) may be constructed using this equation.

It must be emphasized that in deriving eqn. 3.66, and hence the eqns. 4.25 and 4.26, we made the assumption that the solid was a pure phase. This assumption is a reasonably good

*The heat of fusion is often designated by ΔH_f. I have chosen to use the subscript m to avoid confusion with heat of formation, for which we have already been using the subscript f.

Example 4.2 Calculating melting curves

Using the data given below and assuming (1) that the melt is an ideal solution and (2) diopside and anorthite solids are pure phases, calculate a T–X phase diagram for melting of an anorthite–diopside mixture.

	T_m	ΔH_m
	°C	J/mol
Diopside	1391	138100
Anorthite	1553	136400

Data from Stebbins *et al.* (1983).

Answer: Solving eqn. 4.26 for T, and replacing activity with mole fraction (since we may assume ideality), we have:

$$T = \frac{\Delta H_{i,m}}{\frac{\Delta H_{i,m}}{T_{i,m}} - R \ln X_i^l} \tag{4.27}$$

We then calculate T for every value of X_{An} and X_{Di}. This produces two curves on a T–X plot, as shown in Figure 4.9. The curves intersect at the eutectic, or lowest point at which melt may exist in the system.

Comparing our result with the actual phase relationships determined experimentally (Figure 4.8), we see that while the computed phase diagram is similar to the actual one, our computed eutectic occurs at $X_{Di} = 0.70$ and 1335°C and the actual eutectic occurs at $X_{Di} \approx 0.56$ and 1274°C. The difference reflects the failure of the several assumptions we made. First, and most importantly, silicate liquids are not ideal solutions. Second, the entropies and enthalpies of fusion tend to decrease somewhat with decreasing temperature, violating the assumption we made in deriving eqn. 4.26. Third, the diopside crystallizing from anorthite–diopside mixtures is not pure, but contains some Al and an excess of Mg.

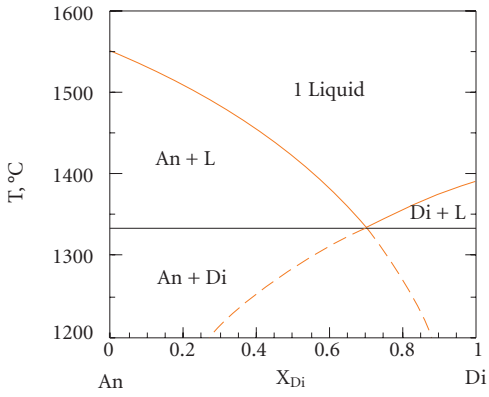

Figure 4.9 Computed phase diagram for the system anorthite–diopside ($CaAl_2Si_2O_8$–$CaMgSi_2O_6$). The eutectic occurs at $X_{Di} = 0.7$ and 1334°C. The dashed lines beyond the eutectic give the apparent melting points of the components in the mixture.

one for ice, and for the anorthite–diopside binary system, but it is not generally valid. Should the solid or solids involved exhibit significant solid solution, this assumption breaks down and these equations are invalid. In that case, melting phase diagrams can still be constructed from thermodynamic equations, but we need to model the solid solution as well as the liquid one. Section 4.4.2.1 illustrates an example (anorthite–albite) where the two solutions can be modeled as ideal.

4.4.2 Thermodynamics of phase diagrams for binary systems

In a one-component system, a phase boundary, such as the melting point, is univariant since at that point two phases coexist and $f = c - \phi + 2 = 1 - 2 + 2 = 1$. Thus specifying

either temperature or pressure fixes the other. A three-phase point, such as the triple point of water, is invariant. Hence simply from knowing that three phases of water coexist (i.e., knowing we are at the triple point), we know the temperature and pressure.

In binary systems, the following phase assemblages are possible according to the Gibbs phase rule (ignoring for the moment gas phases):

	Phases	Free compositional variables
Univariant	2 solids + liquid, 2 liquids + solid, 3 solids or liquids	0
Divariant	1 solid + 1 liquid, 2 solids, 2 liquids	0
Trivariant	1 solid or 1 liquid	1

When a $\bar{G} - X$ diagram is drawn, it is drawn for a specific temperature and pressure, such that $\bar{G} - X$ are isobaric and isothermal. Thus we have already fixed two variables, and the compositions of all phases in univariant and divariant assemblages are fixed by virtue of our having fixed T and P. Only in trivariant systems are we free to choose the composition of a phase on a $\bar{G} - X$ diagram. Figure 4.10 is a schematic diagram of a two-component, one-phase (trivariant) assemblage, in which there is complete solution between component *1* and component *2*. This phase might be either a liquid, or a solid such as plagioclase. The composition of the phase may fall anywhere on the curve. Of course, since this diagram applies only to one temperature, we cannot say from this diagram alone that there will be complete solution at all temperatures.

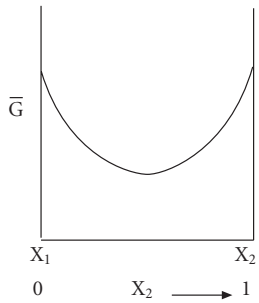

Figure 4.10 Molar free energy vs. composition ($\bar{G} - X_2$) for a one-phase assemblage that exhibits complete solution of either a liquid or solid.

Figure 4.11 illustrates four possible divariant systems. The first case (Figure 4.11a) is that of a liquid solution of composition L' in equilibrium with a solid of fixed composition S_2 (pure component 2). Because the system is divariant, there can be only one possible liquid composition since we have implicitly specified P and T. As usual, the equilibrium

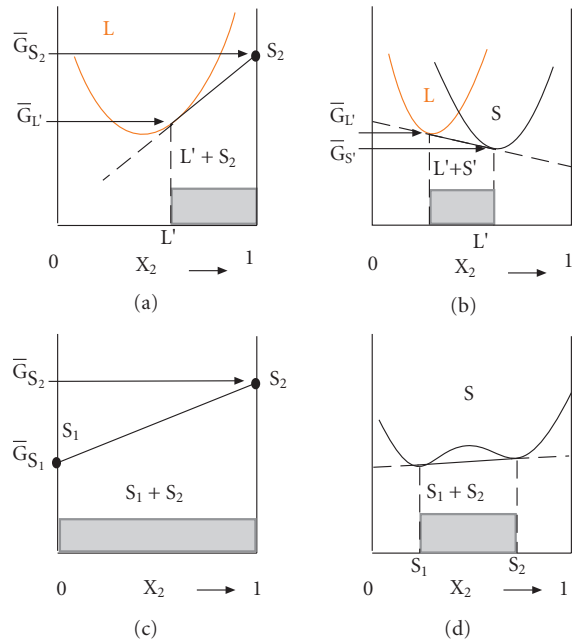

Figure 4.11 Plot of molar free energy vs. composition ($\bar{G} - X_2$) for two-phase divariant systems. (a) A liquid solution (L) is in equilibrium with a solid (S_2) of pure X_2. The shaded area shows the range of composition of systems for which L' and S_2 coexist as separate phases. (b) Here both solid and liquid have variable composition. Equilibrium compositions are determined by finding a tangent to both free energy curves. L' and S' will be the equilibrium phases for systems having compositions in the shaded area. (c) is the case of two immiscible solids, while (d) shows two limited solid solutions of composition S_1 and S_2. Here, the compositions of the solids are given by the point where a straight line is tangent to the curve in two places. After Nordstrom and Munoz (1986). With permission from John Wiley & Sons.

condition is described by $\mu_i^1 = \mu_i^s$ (eqn. 3.17). For $i = 2$, this means the tangent to the free energy curve for the melt must intersect the $X_2 = 1$ line at μ_2^s as shown. In other words, the chemical potential of component 2 in the melt must be equal to the chemical potential of component 2 in the solid. Again, this diagram is valid for only one temperature; at any other temperature, the free energy curve for the liquid would be different, but the composition of this new liquid in equilibrium with solid S_2 would still be found by drawing a tangent from S_2 to the free energy curve of the liquid. At sufficiently high temperature, any tangent would always intersect below S_2. The temperature at which this first occurs is the melting temperature of S_2 (because it is the point at which the free energy of a liquid of pure 2 is less than the solid). The shaded region shows the compositions of systems that will have a combination of solid S_2 and liquid L′ as their equilibrium phases at this temperature.

We can also think of the tangent line as defining the free energy of a mechanical mixture of S_2 and L′. In the range of compositions denoted by the shaded region, this mixture has a lower free energy than the liquid solution, hence at equilibrium we expect to find this mixture rather than the liquid solution.

Figure 4.11b illustrates a system with a liquid plus a solid solution, each of which has its own G–X curve. Again, the equilibrium condition is $\mu_i^l = \mu_i^s$, so the compositions of the coexisting liquid and solid are given by a tangent to both curves. Since the system is divariant and we have fixed P and T, the compositions of the solutions are fixed. All system compositions in the shaded region can be accommodated by a mixture of liquid and solid. Compositions lying to the left of the region would have only a liquid; compositions to the right of the shaded region would be accommodated by a solid solution.

Figure 4.11c illustrates the case of two immiscible solids (pure components 1 and 2). The molar free energy of the system is simply that of a mechanical mixture of S_1 and S_2: a straight line drawn between the free energy points of the two phases.

Figure 4.11d illustrates the case of a limited solution. We have chosen to illustrate a solid solution, but the diagram would apply equally well to the case of two liquids of limited solubility.

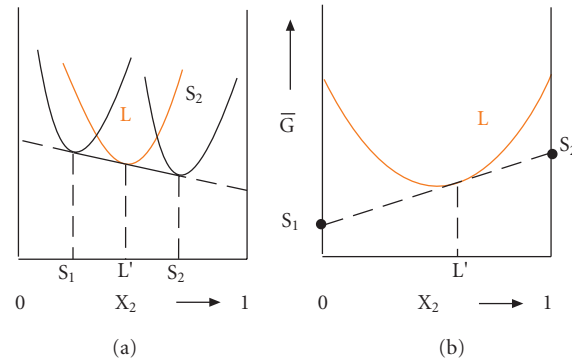

Figure 4.12 Two univariant systems: (a) a liquid plus two solid solutions, and (b) two pure solids and a liquid. Since these systems are univariant, they occur only at one fixed T if P is fixed. After Nordstrom and Munoz (1986). With permission from John Wiley & Sons.

Figure 4.12a shows the case of two solid solutions plus one liquid. The chemical potential of each component in each phase must be equal to the chemical potential of that component in every other phase, so chemical potentials are given by tangents to all three phases. This is a univariant system, so specifying either temperature, pressure, or the composition of a phase fixes other variables in the system. Because of this, if we move to a slightly higher or lower temperature at fixed pressure, one of the phases must be eliminated in a *phase elimination reaction*. If the liquid is the liquid in between the two solids in composition, the reaction is known as a *eutectic*, which is the lowest temperature at which the liquid can exist. Moving to a higher temperature would result in elimination of one of the solids. If, alternatively, the liquid is not between two solids (for example, if the curves L and S_2 in Figure 4.12a were switched), the reaction would be known as a peritectic, and moving to lower temperature eliminates one of the solids. Thus, it is possible for a liquid to persist below a peritectic if the composition is right, but a liquid will never persist at equilibrium below a euctectic. Figure 4.12b is a eutectic in a system where the two solids are the phases of pure components 1 and 2. A line drawn between the free energies of the pure components is also tangential to the liquid curve.

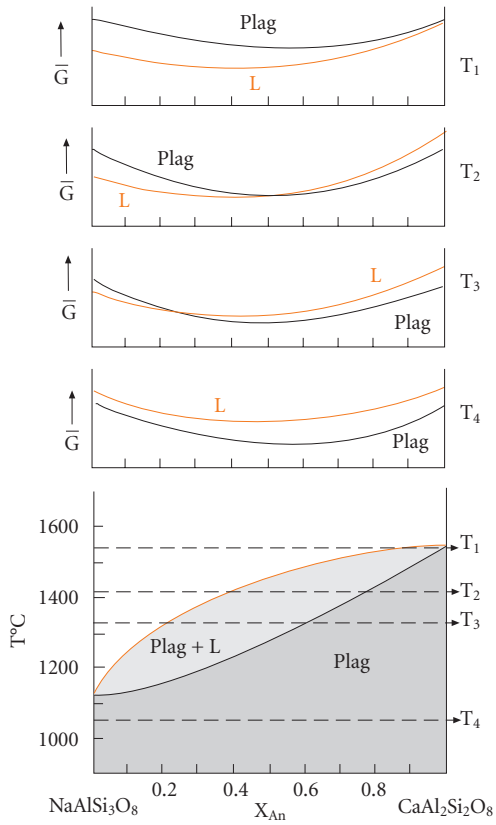

Figure 4.13 G–X diagrams and a T–X phase diagram for the plagioclase–liquid system. From Richardson and McSween (1989). Reproduced with permission.

4.4.2.1 An example of a simple binary system with complete solution: albite–anorthite

Phase diagrams in T–X space can be constructed by analyzing G–X diagrams at a series of temperatures. Let's examine how this can be done in the case of a relatively simple system of two components, albite ($NaAlSi_3O_8$) and anorthite ($CaAl_2Si_2O_8$), whose solid (plagioclase) and liquid exhibit complete solid solution. Figure 4.13 shows G–X diagrams for various temperatures as well as a T–X phase diagram for this system. Since both the solid and liquid exhibit complete solution, we need to consider G–X curves for both.

We start at the highest point at which liquid and solid coexist, T_m (T_1) for anorthite. Here the solid and liquid curves both have the same value at $X_{An} = 1$, and they are at equilibrium. A G–X plot above this temperature would show the curve for the liquid to be everywhere below that of the solid, indicating the liquid to be the stable phase for all compositions.

At a somewhat lower temperature (T_2), we see that the curves for the solid and liquid intersect at some intermediate composition. To the right, the curve for the solid is lower than that of the liquid, and tangents to the solid curve extrapolated to both $X_{Ab} = 1$ and $X_{An} = 1$ are always below the curve for the liquid, indicating the solid is the stable phase. As we move toward *Ab* (left) in composition, tangents to the solid curve eventually touch the curve for the liquid. The point where the tangent touches each curve gives the compositions of the liquid and the solid stable at this temperature. In the compositional range between the points where the tangent touches the two curves, the tangent is below both curves, thus a mechanical mixture of solid and liquid is stable over this compositional range at this temperature. For compositions to the left of the point where the tangent touches the liquid curve, the liquid curve is lower than both the solid curve and a tangent to both, so it is stable relative to both the solid and any mixture of solid and liquid.

Going to progressively lower temperatures (e.g., T_3), the points where a tangent intersects the two curves move toward Ab (to the left). Eventually, at a sufficiently low temperature (T_4), the curve for the solid is everywhere below that of the liquid and only solid solution is stable. By extracting information from G–X curves at a number of temperatures, it is possible to reconstruct the phase diagram shown at the bottom of Figure 4.13.

Since both the solid and liquid show complete miscibility in this system, we will make the simplifying assumption that both solutions are ideal and do an approximate mathematical treatment. We recall that the condition for equilibrium was:

$$\mu_i^{\alpha} = \mu_i^{\beta}$$

We can express the chemical potential of each component in each phase as:

$$\mu_i^{\alpha} = \mu_i^{o\alpha} + RT \ln X_i^{\alpha} \qquad (4.28)$$

Combining these relationships, we have:

$$\mu_{Ab}^{o\ell} - \mu_{Ab}^{os} = RT \ln\left(\frac{X_{Ab}^{s}}{X_{Ab}^{\ell}}\right) \qquad (4.29)$$

and

$$\mu^{o\ell}_{An} - \mu^{os}_{An} = RT \ln\left(\frac{X^s_{An}}{X^\ell_{An}}\right) \qquad (4.30)$$

Here our standard states are the pure end members of the melt and solid. The left side of both of these equations corresponds to the standard free energy change of crystallization, thus:

$$\Delta\bar{G}^{Ab}_m = RT \ln\left(\frac{X^s_{Ab}}{X^\ell_{Ab}}\right) \qquad (4.31)$$

and

$$\Delta\bar{G}^{An}_m = RT \ln\left(\frac{X^s_{An}}{X^\ell_{An}}\right) \qquad (4.32)$$

Both sides of these equations reduce to 0 if and only if $X^\ell_i = X^s_i = 1$ and $T = T_m$. Rearranging:

$$X^s_{Ab} = X^\ell_{Ab} e^{-\Delta\bar{G}^{Ab}_m/RT} \qquad (4.33)$$

$$X^s_{An} = X^\ell_{An} e^{-\Delta\bar{G}^{An}_m/RT} \qquad (4.34)$$

Thus the fraction of each component in the melt can be predicted from the composition of the solid and thermodynamic properties of the end-members. Since $X^\ell_{An} = 1 - X^\ell_{Ab}$ and $X^s_{An} = 1 - X^s_{Ab}$, we can combine eqns. 4.33 and 4.34 to obtain:

$$(1 - X^\ell_{Ab}) e^{-\Delta\bar{G}^{Ab}_m/RT} = 1 - X^\ell_{Ab} e^{-\Delta\bar{G}^{Ab}_m/RT} \qquad (4.35)$$

and rearranging yields:

$$X^\ell_{Ab} = \frac{1 - e^{-\Delta\bar{G}^{An}_m/RT}}{e^{-\Delta\bar{G}^{Ab}_m/RT} - e^{-\Delta\bar{G}^{An}_m/RT}} \qquad (4.36)$$

The point is that *the mole fraction of any component of any phase in this system can be predicted from the thermodynamic properties of the end-members*. We must bear in mind that we have treated this as an ideal system, so we have ignored any G_{excess} term. Nevertheless, the ideal treatment is relatively successful for the plagioclase system. For non-ideal systems, we merely replace mole fraction in the above equations with activity. Provided they are known, interaction parameters can be used to calculate activity coefficients (e.g., eqns. 4.18 or 4.12 as the case may be). Beyond that, non-ideal systems can be treated in a manner exactly analogous to the earlier treatment.

4.5 GEOTHERMOMETRY AND GEOBAROMETRY

An important task in geochemistry is estimating the temperature and pressure at which mineral assemblages equilibrate. The importance extends beyond petrology to tectonics and all of geology because it reveals the conditions under which geological processes occur. Here we take a brief look at the thermodynamics underlying geothermometry and geobarometry (since most reactions are both temperature and pressure dependent, it is perhaps more accurate to use the term "thermobarometer"). We have space to consider just a few relatively simple thermobarometers based on the composition of mineral pairs. Particularly in complex metamorphic systems, modern thermobarometry involves simultaneously solving for the equilibrium among many phases, and requires relatively sophisticated computer algorithms such as PERPLEX (Connolly, 1989) or THERMOCALC (Powell and Holland, 2008). Those approaches, however, involve the same fundamental principles as the simple geobarometers we consider below. Here we focus on "chemical" geobarometers that depend on the distribution of chemical components between phases. In Chapter 9, we will see that temperatures can also be deduced from the distribution of isotopes of an element between phases.

Geothermometry and geobarometry involve two nearly contradictory assumptions. The first is that the mineral assemblage of interest is an equilibrium one, and the second is that the system did not re-equilibrate during the passage through lower P and T conditions that brought the rock to the surface where it could be collected. As we will see in the next chapter, reaction rates depend exponentially on temperature, hence these assumptions are not quite as contradictory as they might seem.

4.5.1 Theoretical considerations

In general, geobarometers and geothermometers make use of the pressure and temperature dependence of the equilibrium constant, K. In Section 3.9 we found that $\Delta G° = -RT$

ln K. Assuming that ΔC_p and ΔV of the reaction are independent of temperature and pressure, we can write:

$$\Delta G^o = \Delta H^o_{T,P_{ref}} - T\Delta S^o_{T,P_{ref}} + \Delta V^o_{T,P_{ref}}(P - P_{ref}) = -RT\ln \mathrm{K} \quad (4.37)$$

where the standard state of all components is taken as the pure phase at the temperature and pressure of interest, and the enthalpy, entropy and volume changes are for the temperature of interest and a reference pressure (generally 0.1 MPa).

Solving eqn. 4.37 for ln K and differentiating the resulting equation with respect to temperature and pressure leads to the following relations:

$$\left(\frac{\partial \ln K}{\partial T}\right)_P = \frac{\Delta H^o_{T,P_{ref}} + \Delta V^o_{T,P_{ref}}(P - P_{ref})}{RT^2} \quad (4.38)$$

and

$$\left(\frac{\partial \ln \mathrm{K}}{\partial P}\right)_T = \frac{\Delta V^o_{T,P_{ref}}}{RT} \quad (4.39)$$

These equations provide us with the criteria for reactions that will make good geothermometers and geobarometers. For a good geothermometer, we want the equilibrium constant to depend heavily on T, but be approximately independent of P. Looking at eqn. 4.38, we see this means the ΔH term should be as large as possible and the ΔV term as small as possible. A fair amount of effort was devoted to the development of a geothermometer based on the exchange of Fe and Mg between olivine and pyroxenes in the late 1960s. The effort was abandoned when it was shown that the ΔH for this reaction was very small. As a rule, a reaction should have a $\Delta H°$ of at least 1 kJ to be a useful geothermometer. For a good geobarometer, we want the ΔV term to be as large as possible. Even though the rhodonite ($[Mn,Fe,Ca]SiO_3$) and pyroxmangite ($[Mn,Fe]SiO_3$) pairs commonly occur in metamorphic rocks, the reaction rhodonite → pyroxmangite does not make a useful geobarometer because the ΔV of reaction is only 0.2 cc/mol. In general, a reaction should have a ΔV of greater than 2 cc/mol if it is to be used for geobarometry.

The following discussion presents a few examples of useful chemical geothermometers and geobarometers. It is not an exhaustive treatment, nor should it be inferred that those examples discussed are in any way superior to other geothermometers and geobarometers. Reviews by Essene (1989), Putirka (2008), Anderson *et al*. (2008), Blundy and Cashman (2008), and Powell and Holland (2008) summarize a wide range of igneous and metamorphic thermobarometers.

4.5.2 Practical thermobarometers

4.5.2.1 Univariant reactions and displaced equilibria

We can broadly distinguish three main types of thermobarometers. The first is the *univariant reaction*, in which the phases have fixed compositions. They are by far the simplest, and often make good geobarometers as the ΔV of such reactions is often large. Examples include the graphite–diamond transition, any of the SiO_2 transitions (Figure 4.7), and the transformations of Al_2SiO_5, shown in Figure 4.14. While such thermobarometers are simple, their utility for estimating temperature and pressure is limited. This is because exact temperatures and pressures can be obtained only if two or more phases coexist, for example, kyanite and andalusite in Figure 4.14. If kyanite and andalusite are both found

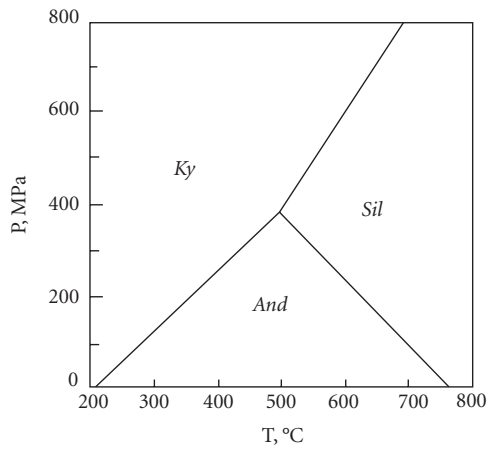

Figure 4.14 Phase diagram for Al_2SiO_5 (kyanite–sillimanite–andalusite) as determined by Holdaway (1971). Reprinted by permission of the American Journal of Science.

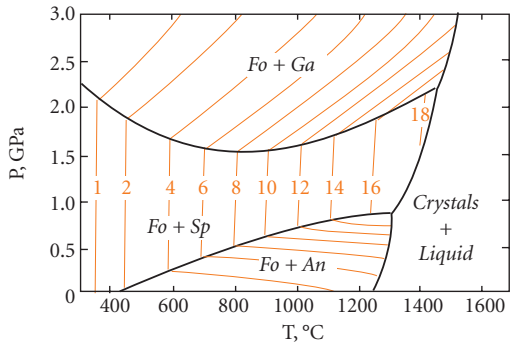

Figure 4.15 Isopleths of Al in orthopyroxene (thin red lines; weight percent) coexisting with forsterite plus an aluminous phase in the CMAS (Ca-Mg-Al-Si) system. After Gasparik (1984b). With permission from Elsevier.

in a rock, we can determine either temperature or pressure if we can independently determine the other. Where three phases, kyanite, sillimanite, and andalusite, coexist the system is invariant and P and T are fixed. If only one phase occurs, for example sillimanite, we can only set a range of values for temperature and pressure. Unfortunately, the latter case, where only one phase is present, is the most likely situation. It is extremely rare that kyanite, sillimanite, and andalusite occur together.

The term *displaced equilibria* refers to variations in the temperature and pressure of a reaction that result from appreciable solution in one or more phases. Thermobarometers based on this phenomenon are more useful than univariant reactions because the assemblage can coexist over a wide range of P and T conditions. In the example shown in Figure 4.15, the boundaries between garnet-bearing, spinel-bearing, and plagioclase-bearing assemblages are curved, or "displaced" as a result of the solubility of Al in enstatite. In addition to the experimental calibration, determination of P and T from displaced equilibria requires (1) careful determination of phase composition and (2) an accurate solution model.

Geobarometers based on the solubility of Al in pyroxenes have been the subject of extensive experimental investigations. The general principle is illustrated in Figure 4.15, which shows the concentration of Al in orthopyroxene (opx) coexisting with olivine (forsterite) and an aluminous phase, anorthite, spinel, or garnet. The Al content of opx depends almost exclusively on pressure in the presence of anorthite, is essentially independent of pressure in the presence of spinel, and depends on both temperature and pressure in the presence of garnet. Orthopyroxene–garnet equilibrium has proved to be a particularly useful geobarometer.

Garnet is an extremely dense phase. So we might guess that the ΔV of reactions that form it will be comparatively large, and therefore that it is potentially a good geobarometer. The concentration of Al in opx in equilibrium with garnet may be used as a geobarometer if temperature can be independently determined. Although there has been a good deal of subsequent work and refinement of this geobarometer, the underlying thermodynamic principles are perhaps best illustrated by considering the original work of Wood and Banno (1973).

Wood and Banno (1973) considered the following reaction:

$$Mg_2Si_2O_6 + MgAl_2SiO_6 \rightleftharpoons Mg_3Al_2Si_3O_{12} \quad (4.40)$$

opx solid solution $\rightleftharpoons$ pyrope garnet

In developing a geobarometer based on this reaction, they had to overcome a number of problems. First, the substitution of Al in orthopyroxene is a coupled substitution. For each atom of Al substituting in the M1* octahedral site, there must be another Al atom substituting for SiO_2 in the tetrahedral site. Second, there was a total lack of thermodynamic data on the $MgAl_2SiO_6$ phase component. Data was lacking for a good reason: the phase does not exist and cannot be synthesized as a pure phase. Another problem was the apparent non-ideal behavior of the system, which was indicated by orthopyroxenes in Fe- and Ca-bearing systems containing less alumina than in pure MgO systems at the same pressure.

* The two octahedral sites in pyroxene normally occupied by metal ions such as Mg, Fe, and Ca are slightly different; the smaller of the two is labeled M1 and the larger of the two, occupied by Ca in diopside, is labeled M2.